Journal of Power Sources 247 (2014) 339–345

Contents lists available at ScienceDirect

Journal of Power Sources

journal homepage: www.elsevier.com/locate/jpowsour

# Influence of air contaminants on planar, self-breathing hydrogen PEM fuel cells in an outdoor environment

Johannes Biesdorf, Nada Zamel, Timo Kurz*

*Fraunhofer Institute for Solar Energy Systems (ISE), Freiburg, Germany*

## HIGHLIGHTS

- Development of an outdoor test bench for parallel operation of 30 fuel cell modules.
- Continuous operation of 90 fuel cell modules for over 4500 h at three sites.
- Influence of different contamination levels on cell performance is analyzed.
- Reversible degradation due to air contaminants is presented and analyzed.

## ARTICLE INFO

*Article history:*
Received 7 January 2013
Received in revised form
7 August 2013
Accepted 16 August 2013
Available online 7 September 2013

*Keywords:*
Air contaminants
PEM fuel cells
Field study
Reversible/irreversible degradation
Long-term operation

## ABSTRACT

In this study, the effects of air contaminants on the operation of air-breathing fuel cells in an outdoor environment are investigated. For this purpose, a unique testing platform, which allows continuous operation of 30 cells at different locations, was developed. Three of these testing platforms were placed at different sites in Freiburg im Breisgau, Germany, with high variances of weather and pollution patterns. These locations range from a highly polluted place next to a busy highway to a location with virtually pure air at an altitude of 1205 m. The fuel cells were tested at all sites for over 4500 h in continuous operation. The degradation of the cells due to air pollutants was measured as a voltage decrease for three different operation loads and membranes from two different manufactures. As the temperature of the fuel cells has not been regulated, the irreversible degradation of the cell voltages could not be isolated from the dominant influence of the temperature in the raw data. With the use of the measured data, the impact of real mixtures of air contaminants was observed to be mainly reversible.



## 1. Introduction

With the push towards the commercialization of polymer electrolyte membrane (PEM) fuel cells, especially for automotive applications, the overall price of the system must be taken into account. For this purpose, the oxidant of choice becomes ambient air, which aside from $N_2$ and $O_2$ can also consist of various compounds such as, $NO_x$, $SO_2$, $H_2S$ and $CO_x$. The presence of these compounds in the oxidant stream of PEM fuel cells can severely affect their performance.

Extensive laboratory studies on the effect of such contaminants are available in literature. Contamination by nitrogen oxides (eg. NO, $NO_2$) has been evaluated in Refs. [1–7]. From these studies, it becomes clear that contamination by high concentrations of nitrogen oxides can lead to irreversible degradation of the cell voltage. Recovery of the performance of cells exposed to low concentrations can be obtained with the supply of neat air where the required recovery time is highly dependent on the concentration of $NO_x$ and is much longer than the poisoning time. The contamination of the cathode by these oxides was found by Refs. [1,2] to not be catalytic, but rather is a catalyst–ionomer interface contamination. In Ref. [1], this conclusion was based on cyclic voltammetry (CV) measurements during $NO_2$ exposure. From the measurements, Mohtadi et al. hypothesized that the decrease in the oxygen reduction reaction (ORR) rate can be attributed to $NO_2$ being adsorbed and subsequently electrochemically reduced on the cathode. The product of such a reaction is $NH_4^+$, which is a well known poison of the ionomer. In Ref. [2], the authors proposed that NO reacts readily with oxygen to form $NO_2$, which in turn can react with water to form nitrous acid ($HNO_2$). With $HNO_2$ being relatively unstable, it can react with oxygen to form nitric acid, $HNO_3$. The latter reaction results in the release of protons under wet conditions; hence, increasing the overpotential of the cathode tremendously.

* Corresponding author.
*E-mail addresses:* timo.kurz@ise.fraunhofer.de, kurzwielang@gmx.de (T. Kurz).

0378-7753/$ – see front matter © 2013 Elsevier B.V. All rights reserved.
http://dx.doi.org/10.1016/j.jpowsour.2013.08.064

Other commonly investigated contaminants of the cathode are sulfur compounds (eg. $SO_2$, $H_2S$). This contamination directly affects the catalyst, as the sulfur species strongly adsorb on the platinum sites preventing the reduction of oxygen. This adsorption reaction has been studied intensively in Refs. [1,8]. Recovery has been observed once the supply of $H_2S$ was shut off and neat air was used as the oxidant. Mitigation of contamination by sulfur dioxide was observed in Ref. [8] when the humidification of the air stream was increased. This is mainly attributed to the high solubility of $SO_2$ in water.

In the above mentioned papers, the effects of single contaminants are elaborated. For real applications with ambient air, tests with realistic gas mixtures have to be carried out. Jing et al. [9] present measurements in the laboratory with a mixture of several contaminants (see Table 1). They observed, that the cell voltage decreases by about 160 mV during 120 h of operation. After CV scanning, the voltage quickly recovers to 94% of its original value. From their findings, they suggested that the adsorption reaction of $NO_2$ is given priority in the presence of sulfur compounds, so that they attributed the drop in the cell performance in the presence of $NO_2$ to this contaminant. Knights et al. [10] analyzed gas mixtures of $H_2S$, $NO_2$ and $SO_2$ (see Table 1), concluding that the loss in cell performance is simply the additive result of each single contaminant.

Although mixtures of air with several contaminants are investigated in previous studies [9,10], they are far above realistic concentrations (see location L1–3 in Table 1). Consequently, the effects of the lower impurity concentrations in real ambient air on the long term degradation of fuel cells have not been evaluated so far. Hence, the objective of the present field study is to investigate the influence of air contaminants on planar, self-breathing PEM fuel cells in an outdoor environment. Therefore, neither the temperature nor the humidification is regulated within the cells. The test stands were placed at three different locations around Freiburg im Breisgau, Germany, each of them carrying 30 air-breathing fuel cell modules. Since the supplied hydrogen was pure (purity 5.0), degradation of the anode due to contamination from the hydrogen feed could be suspended. Thus, the coupled influence of temperature and contamination of the air feed on the cell voltage could be examined.

## 2. Experimental

### 2.1. Locations

The following three locations were chosen in order to achieve a high variance in contamination levels. Table 1 compares the average of $NO_x$, CO and $SO_x$ concentrations and the standard deviations of the concentration fluctuations at the three sites:

**Table 1**
Comparison of different pollutant mixtures in literature and at three different locations in Freiburg im Breisgau, Germany. Also the amplitudes of impurity concentration variations, measured in terms of the standard deviation, at location 1–3 are given. As can be seen, the gas mixtures analyzed in Refs. [9,10] are more than 4 times higher than in our field study. Some pollutant concentrations were not measured at all locations.

| | Pollutant concentration/ppb | | | | | | | |
|---|---|---|---|---|---|---|---|---|
| | Average values | | | | Standard deviation | | | |
| | $SO_2$ | NO | $NO_2$ | CO | $SO_2$ | NO | $NO_2$ | CO |
| Jing et al. [9] | 1000 | 200 | 800 | – | – | – | – | – |
| Knights et al. [10] | 5000 | – | 5000 | – | – | – | – | – |
| Location 1 | – | 63.6 | 32.7 | 361.7 | – | 61.4 | 21.2 | 198.0 |
| Location 2 | – | – | 15.8 | – | – | – | 5.1 | – |
| Location 3 | 0.1 | 0.2 | 0.6 | 112.0 | 0.2 | 0.6 | 0.8 | 28.0 |

1. The highly polluted site (L1) is located next to a city highway with approximately 48 700 vehicles passing per day, out of which 7% are lorries [11]. High concentrations of contaminants are measured due to the exhausts of combustion engines and the abrasion of automotive components from tyres or during breaking. Thus, at this location the cells could be expected to be strongly influenced by air contamination. A weather station by the State Agency for Environment, Measurements and Nature Conservation Baden Württemberg (LUBW), situated in the immediate vicinity of the test stand, measures concentrations of air pollutants.
2. The second location (L2) resides in an urban environment in the neighborhood of the main train station of Freiburg im Breisgau. The adjacent road is mostly used by passenger vehicles. Weather and contamination data are recorded by the Deutscher Wetterdienst (DWD) [12]. The location shows moderate contamination levels.
3. The third location (L3) is the least polluted and is situated on a mountain at an altitude of 1205 m [13]. The temperature at this location usually is 5 °C lower, resulting in higher average relative humidities ($\approx$90% RH) in comparison to the two urban locations L1 and L2 ($\approx$75% RH). Furthermore, concentrations of air pollutants are very low. They are measured by the Umweltbundesamt (UBA) (Federal Environmental Agency).

### 2.2. Experimental setup

The experimental setup is shown in Fig. 1. Each test platform is composed of a gas bottle locker and a control unit. The gas bottle compartment contains two 50 l/200 bar hydrogen bottles and safety components. This setup allows the continuous operation of the fuel cells with the only interruption during change of the gas bottles every two weeks. The control unit includes the measurement box containing 30 fuel cells and provides the automated operation of the fuel cells and data acquisition through a LabView software.

Within the fuel cell box (see Fig. 1), 30 fuel cell modules are placed vertically in the air stream, which is provided by two axial fans. The modules are arranged in six groups of five identical modules. Membrane electrode assemblies from two different manufactures are used, and three different operating points are determined by ohmic load resistors of 15 Ω, 1 Ω and 0.56 Ω.

The modules are supplied in parallel with hydrogen (purity 5.0) at 200 mbar overpressure. The anode outlets of every group end in a common purge valve and water collecting tank. The temperature of the inlet air stream is not regulated. Only when ambient conditions reach a temperature of less than 0 °C, electrical heaters are used to prevent the fuel cells from freezing. The cell temperatures are measured at the housing of one cell per group. Temperature and relative humidity of the inlet air stream are measured as well as the hydrogen content of the outlet air for safety reasons.

The fuel cell modules (see Fig. 2) are composed of two single cells connected in series (planar). The cells are assembled in an injection-molded housing with an active surface area of 5.5 $cm^2$ per cell. Hydrogen is supplied by serpentine flow channels to the anode, and the ambient air reaches the cathode by diffusion through the gas diffusion layer (GDL). Both MEA types have the same GDLs, which are supplied by Freudenberg (H2315 I3 C1), including a microporous layer (MPL) with a common thickness of 270 μm. The actual types of membranes are confidential and cannot be disclosed in this publication. However, both membranes have the same thickness of 30 μm. The first type (MEA I) is assembled as a membrane with two gas diffusion layers bearing the catalyst layers (gas diffusion electrodes). The second type (MEA II) is assembled as a membrane electrode assembly plus gas diffusion layers.

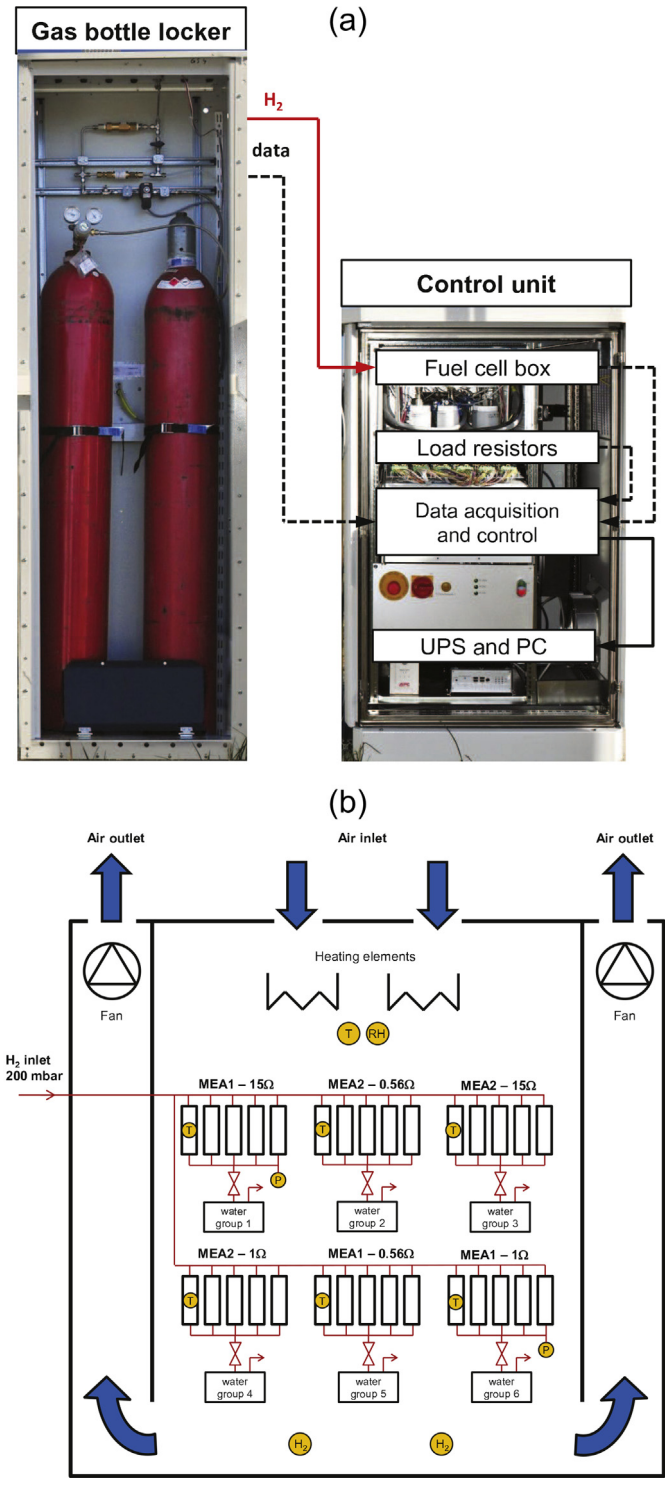


**Fig. 1.** (a) Schematic of the test equipment. The gas bottle locker includes two hydrogen bottles of 50 l at 200 bar. The control unit contains the 30 fuel cell modules and provides the automated operation and data acquisition. (b) Schematic of the fuel cell box containing 30 planar, self-breathing fuel cell modules. The hydrogen is provided from the gas bottle locker, whereas oxygen diffuses into the open cathode GDLs from an air stream generated by two fans. Heaters in the air inlet prevent the fuel cell modules from freezing below 0° C ambient temperature.

## 3. Results and discussion

The three different load resistors were chosen in order to investigate the effects of pollutants in three different regions of the

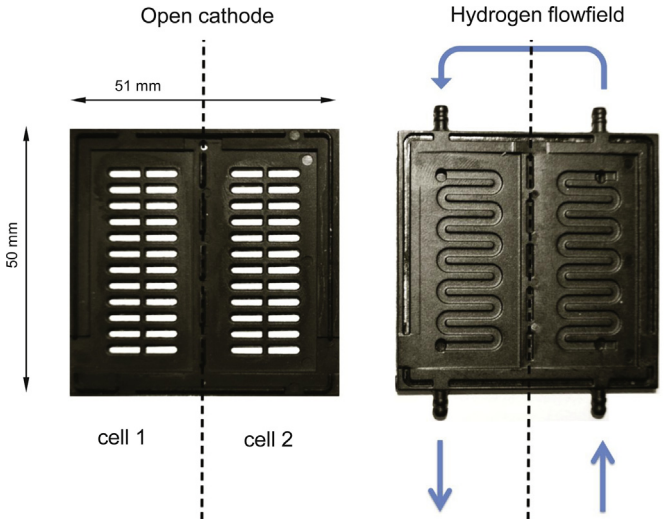


**Fig. 2.** Illustration of the fuel cell modules composed of two single cells. On the anode site, hydrogen is provided through serpentine flow channels. Oxygen from the ambient air diffuses into the open cathode GDL.

voltage–current characteristic (see Fig. 3). The first operating point with an ohmic resistance of $R = 15\ \Omega$ is situated at the junction of the kinetic activation region with the ohmic loss region at about 25 mA cm$^{-2}$. At this point, the influence of pollutants on the cell voltage at low reaction rates can be analyzed. The second operating point with $R = 1\ \Omega$ corresponds to a current density of approximately 170 mA cm$^{-2}$, representing a moderate operation within the ohmic loss region. The third operating point with $R = 0.56\ \Omega$ at a current density of about 270 mA cm$^{-2}$ is situated in the region where mass transport losses begin to dominate.

From the investigations at these three operating points, a comprehensive understanding of the effects of air contaminants on the cell voltage can be deduced taking into account different membrane and operating point effects.

### 3.1. Raw data

Fig. 4(a) shows the cell voltage of three different fuel cell modules during a period from October 2011 (0 h) to April 2012 (4500 h) at L1. The voltages show a high variation, most dominant at the highest load of $R = 0.56\ \Omega$. It decreases until February

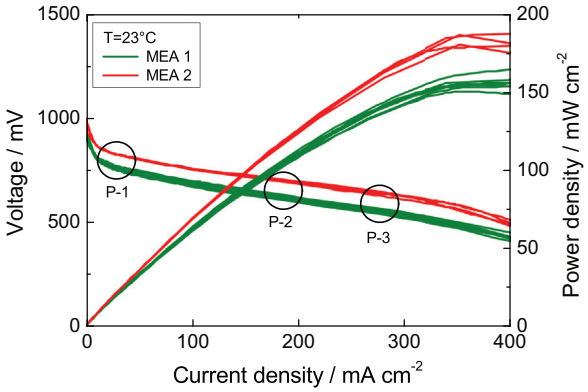


**Fig. 3.** Polarization curves of the two different fuel cell modules with different MEAs. For the investigation of the effects of pollutants, three different load points were chosen for long term testing: P-1 ≈ 25 mA cm$^{-2}$ (load resistance $R = 15\ \Omega$), P-2 ≈ 170 mA cm$^{-2}$ (load resistance $R = 1\ \Omega$) and P-3 ≈ 270 mA cm$^{-2}$ (load resistance $R = 0.56\ \Omega$).

(3000 h) and increases again until April. The voltage characteristic shows a high accordance with the temperature, which suggests a close functional relationship between both. Regarding daily variations of the cell voltage and temperature (see Fig. 4(b)), a nearly analog correlation can be observed. This positive correlation can be explained by the following effects:

- The kinetics of both oxygen reduction reaction (ORR) and hydrogen oxidation reaction (HOR) are strongly influenced by temperature. According to the Butler–Volmer equation, a higher temperature reduces the overpotential and increases the cell voltage.
- The conductivity of the membrane increases with higher temperature. This is mainly due to the increase in proton mobility with the help of the side groups of the polymer.

Although ambient humidity can also influence the membrane conductivity during operation, from Fig. 4(a) and (b), a rather higher correlation between the temperature and voltage is shown. This is due to the passive cathode of the cell, where mass transport problems dominate the overall voltage loss rather than their ohmic counterparts.

- The total amount and distribution of water in the gas diffusion layers are also affected by temperature. Condensation and evaporation rates depend on the temperature and humidity of the air flow, and on the temperature inside the cell. Since the water content of the GDL affects mass transport losses, the cell voltage will be influenced by changes in the water content due to temperature variations.

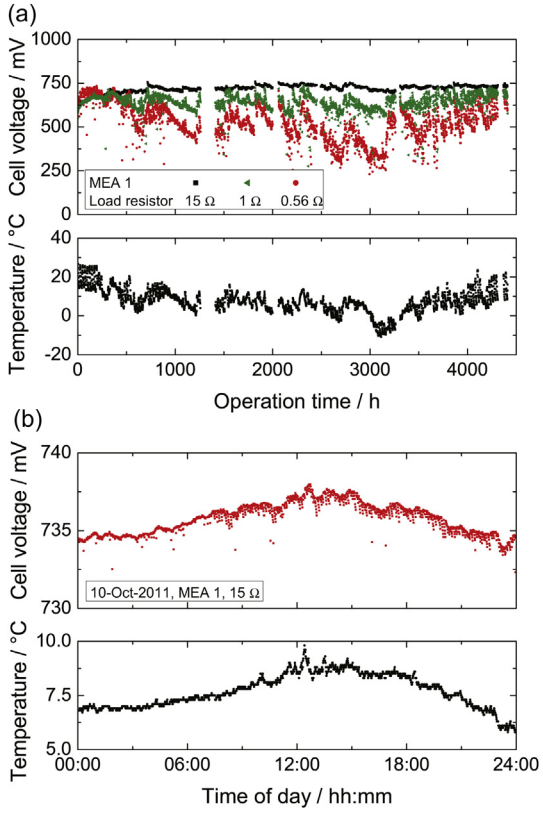


**Fig. 4.** (a) Long term evolution of the ambient temperature and the cell voltage at three different load points at L1. (b) Daily variation of the ambient temperature and the cell voltage at low current densities ($R = 15\ \Omega$) at location L3.

- The amount and distribution of product water in the gas diffusion layers are also affected by the temperature. Condensation and evaporation rates depend on the temperature and humidity of the air flow, and on the temperature inside the cell. Since the water content of the GDL affects mass transport losses, the cell voltage will be influenced by changes in the water content due to temperature variations.

These changes in the cell voltage due to temperature variations can superimpose the reversible or irreversible degradation effects due to air contamination. The latter source of temperature influence strongly depends on the operating point: A minor load resistance leads to a higher water production, causing higher mass transport losses. Consequently, investigations about degradation (see Section 3.3) are focused on fuel cells operating with the highest load resistance.

### 3.2. Activation and voltage levels

Fig. 5 plots the temporal evolution of the average voltages of groups with a load of $R = 15\ \Omega$ for MEA 2 at all three locations. Except for L2, the voltage curves show a sharp increase in the first days indicating an activation process of the cells. At location L2, the cells were operated before for two days in laboratory, thus no activation is visible here. The activation rate at the different locations shows no clear trend, so a correlation between activation and air contamination cannot be assumed.

The average cell voltage levels at the different locations show an obvious difference: They increase in the order L1 < L2 < L3, which is the order of decreasing air pollution. This trend is also visible in Table 2. It shows the average cell voltages additionally at all locations, for all three operating points and both MEA types. The voltages are time-averaged over the period between 1500 h and 4500 h of operation. For each load resistance and MEA type, the average cell voltages increase with decreasing air contamination level. One of two values which do not follow this trend is the value of 442 mV for MEA 1, $R = 1\ \Omega$ at L2. The reason for this reduced value was a defect of the purge valve, which led to flooding of the anode compartment for approximately one week. The second exception is the value of 233 mV for MEA 1, $R = 0.56\ \Omega$ at L1. Here, the reason was the formation of pinholes in the membrane, which were detected ex-situ by leakage test.

The observed trend is even more significant if the average temperature is taken into account. It is approximately 5 °C lower at the mountain location L3 than at L1 and L2. From the temperature

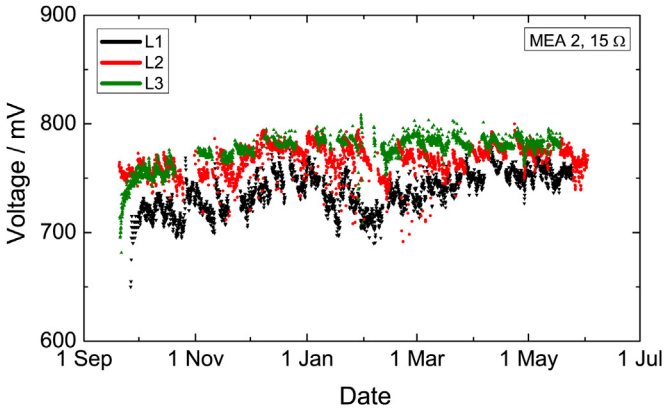


**Fig. 5.** Comparison of the cell voltage evolution at the three different locations. The least polluted location L3 shows increased average voltages compared to the more contaminated locations L1 and L2.

**Table 2**
Averaged cell voltages at three different locations for both MEA types and three different load points. At the least polluted location L3, the highest cell voltages can be measured.

| Cell voltage/mV | | | | | | |
|---|---|---|---|---|---|---|
| Location | 15 Ω | | 1 Ω | | 0.56 Ω | |
| | MEA 1 | MEA 2 | MEA 1 | MEA 2 | MEA 1 | MEA 2 |
| L1 | 694 | 738 | 637 | 649 | 233 | 527 |
| L2 | 721 | 757 | 442 | 672 | 572 | 567 |
| L3 | 754 | 780 | 646 | 693 | 631 | 581 |

influence alone, the cell voltages could be expected to be lowest at L3, but apparently the influence of air contamination outweighs the temperature influence, leading to highest voltage levels at location L3.

### 3.3. Degradation

In the following section, we distinguish between reversible and irreversible degradation effects. Reversible degradation is considered to be mainly caused by reversible catalyst poisoning, while irreversible degradation is considered to occur due to the aging of cell components and permanent reduction of the active surface area of the catalyst.

#### 3.3.1. Reversible degradation

In the following, the reversible degradation of the cell voltages is investigated and related to variations in the concentrations of air impurities. Our findings cannot be compared with the accelerated laboratory experiments presented in the introduction, because there, pollutant concentrations are one or two orders of magnitude higher (see Table 1).

In present study, a distinction between the influences of different air contaminants could not be made, because their variations were very concordant. The concentration levels of all measured impurities show daily oscillations with low values during the nights and higher levels of contamination during the day. Therefore, reversible degradation effects to the entire mixture of contaminants in the ambient air are attributed.

In order to examine reversible degradation effects, Fig. 6 shows the variations of $NO_x$ concentrations and the cell voltage at low load ($R = 15\ \Omega$) at location L1 for representative time periods of one month (a) and one week (b). A negative correlation between cell voltage and $NO_x$ concentrations is clearly visible in the graphs. Location L1 is directly situated next to a city highway, so that air pollutant concentrations highly depend on the volume of traffic, which is large during the day and low during the night. Accordingly, the cell voltage is low during the day, but as impurity concentrations decrease during the night, the cell voltage recovers. A similar analysis holds for the weekly cycles with low impurity concentrations and higher cell voltages during the weekends with low traffic volume. Thus, we observe a reversible negative influence of air impurities on the cell voltage. It should be emphasized again that NO and $NO_2$ only serve as examples for the pollutants mixture which is present at location L1, because the daily variations of the concentrations of all contaminants, including also $SO_2$ and CO, are highly correlated.

The variations of air impurity concentrations and air temperature are quite concordant: during the night, temperatures are generally low, and, due to the low volume of traffic, the air pollution levels as well. The opposite is true during the day. Since both temperature and impurities have opposing influences on the cell voltage, the effects of both cancel each other to a certain extent,

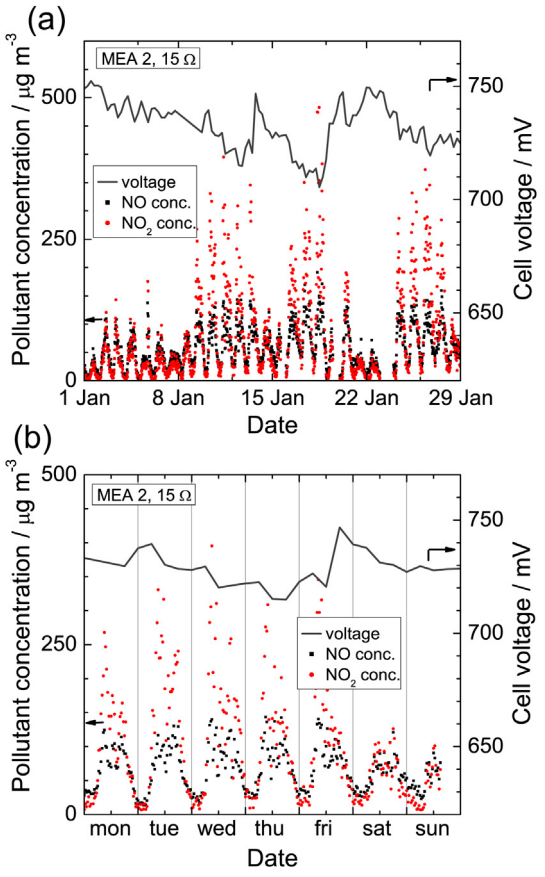


**Fig. 6.** Impact of pollutants on the raw cell voltages at location L1 with a load resistor of 15 Ω for two time periods: (a) one month; (b) one week. The cell voltage decreases with increasing pollutant concentration, but recovers reversibly at lower concentrations during the night.

so that the decrease in the cell voltage with increasing impurity concentrations during the day is partly counterbalanced by the positive effect of rising temperatures. However, the cell voltages oscillate in opposition to the $NO_x$ concentrations, which means that for low current densities (load resistance $R = 15\ \Omega$) and high-amplitude variations of air pollutant concentrations, the influence on the cell voltage of the latter dominates over the influence of the daily temperature variations.

In the following, we will analyze the competing effects of air temperature and air pollutants on the cell voltage in more detail. Fig. 7 compares the variations of the voltages of one cell at low load (load resistance $R = 15\ \Omega$) with another cell at high load (load resistance $R = 0.56\ \Omega$) at the strongly polluted location L1. In the lower part of the figure, the variations of the cell temperature and the $NO_x$ concentrations are shown. Every 6 h, temperature ramps (increase of ≈4 °C during 15 min) of the inlet air have been executed in order to adjust a temperature–voltage model. It should be noted that variations of the ambient air temperature translate one-to-one to variations of the cell temperature. It is clearly visible that the cell voltage for high load (blue line in the web version) directly follows the evolution of the cell temperature, whereas the cell voltage for low load (gray line) evolves inversely to the pollutant concentrations. We can conclude that for high amplitudes of contaminant concentration variations, as is the case at location L1 (see Table 1), the evolution of the cell voltage at low load is dominated by these variations. Conversely, for high load the effect of the temperature fluctuations dominates and masks the opposing contamination effect. This can be explained with the strong

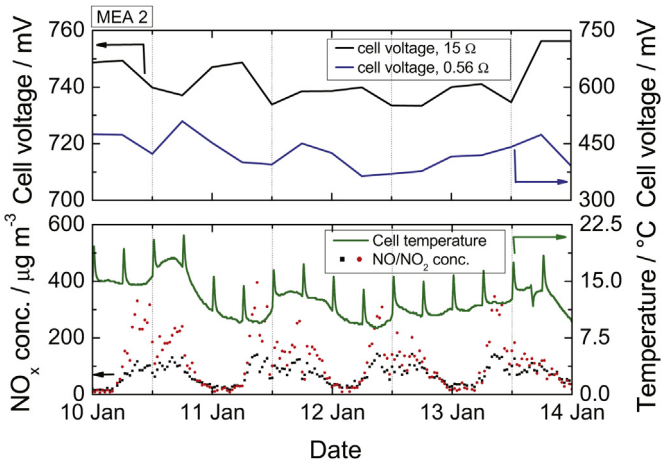


**Fig. 7.** Evolution of the cell voltage at different load points. At low current densities a high influence of air impurities is visible, while this influence is masked at higher current densities by the effect of temperature variations.

influence of the water content on the cell voltage at high load, where mass transport losses become increasingly important, which makes the cell voltage highly sensitive to temperature variations.

To analyze the influence of the different effects and contamination sources (NO, $NO_2$, CO), we calculate correlation coefficients (Pearson product–moment correlation coefficient) of the different quantities with the cell voltage. The correlation coefficient serves as a measure of the degree of linearity between the cell voltage and measured variable. A coefficient of nearly ±1 means a high (positive or negative) linear dependency, 0 means no linear dependency. A time interval of single days has been chosen to have enough points of measurement to correlate, but also having an adequate small number to minimize the influence of irreversible degradation.

The results of the dimensionless coefficients are plotted as average values of approximately 130 days in Fig. 8 for two locations, L1 (a) and L3 (b).

Fig. 8 compares the correlation coefficients between the daily cell voltage variations and the daily variations of the concentrations of NO, $NO_2$ and CO as well as the cell temperature for the two different locations L1 (a) and L3 (b) (compare Table 1). The values shown are averaged over approximately 130 days.

The correlation coefficients in (a) confirm the results discussed above. With increasing load, the correlation coefficient between cell voltage and cell temperature increases to a positive correlation of more than 0.5 for $R = 0.56\ \Omega$, MEA2. The significantly lower correlation coefficient for $R = 0.56\ \Omega$, MEA1, can be explained with the formation of pinholes in the membrane and the consequent failure of the cells (see Section 3.2). Conversely, the cells with highest load ($R = 0.56\ \Omega$) show no correlation with the pollutant concentrations, but for $R = 15\ \Omega$, a significant negative correlation is given. Here, the negative correlation with CO is strongest, but the difference to NO and $NO_2$ is too small to conclude that CO is the most influential of these pollutants. It should be kept in mind that a negative correlation coefficient between the daily variations of the cell voltage and contaminant concentrations indicates reversible degradation, because it implies that the cell voltage recovers at least partly once the pollutant concentrations decrease towards the night. No recovery of the cell voltage, and thus purely irreversible degradation, would result in a zero correlation coefficient.

A different conclusion can be drawn at location L3 with very low levels of air contamination. The correlation coefficients in Fig. 8(b) show a strong positive correlation of the cell voltages with the cell temperature for all loads. The positive correlation coefficients with

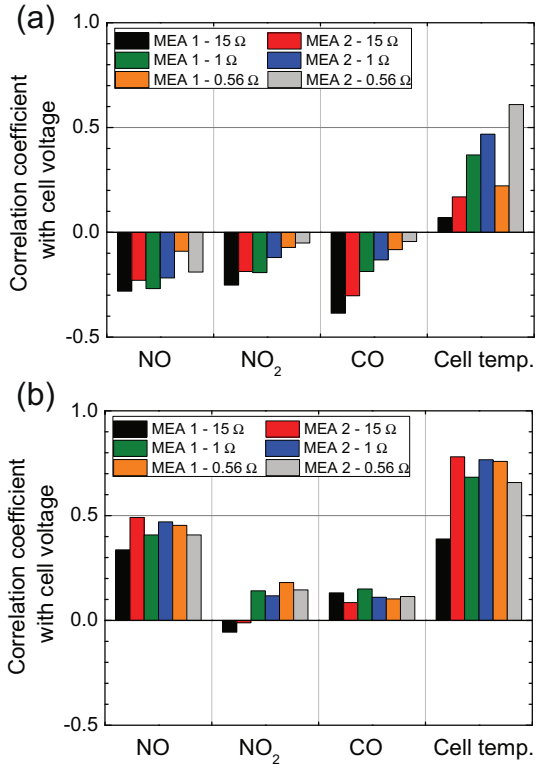


**Fig. 8.** Correlation coefficients between the daily variations of the cell voltage and the daily variations of NO, $NO_2$, CO concentrations and cell temperature at (a) location L1; (b) location L3.

the contaminants are confusing at first sight. They can be explained by the fact, that even though the levels of air contamination at L3 are too low to have an influence on the cell voltage, the pollutant concentrations still show slight daily variations in concordance with the ambient air temperature and thus the cell temperature. The strong positive correlation between cell voltage and cell temperature also leads to a numerically positive correlation coefficient between cell voltage and pollutant concentrations, even though this does not indicate any direct cause and effect relationship. In contrast, this positive correlation must be seen as an indirect correlation via the daily temperature variations. To conclude, for such low air contamination levels as at location L3, the reversible variations of the cell voltages are mainly caused by temperature variations, and the effects of pollutants are masked and negligible.

In summary, the results from the field test clearly show reversible degradation due to the presence of ambient contaminant mixtures. However, the relative importance of reversible contamination effects as compared to the influence of ambient temperature variations depends strongly on the operation point of the fuel cells as well as on the absolute amplitude of the variations in the air pollutant concentrations.

### 3.3.2. Irreversible degradation

As shown in Figs. 4(a) and 5, a clear voltage decrease showing irreversible degradation is not visible because the cell voltage is strongly affected by temperature variations, especially at high loads ($R = 0.56\ \Omega$ and $1\ \Omega$). Calculating a linear fit of the cell voltage with lowest load ($R = 15\ \Omega$, see Fig. 4(a)) between 1500 h (after activation is definitely completed) and 4500 h at location L1, a degradation rate of 1.5 µV $h^{-1}$ is obtained. This rate is in the range of other publicated degradation rates in the laboratory, but still quite low. The reason for that can be that the temperature influence during

the year cannot be fully neglected. On average, in the time interval chosen for this analysis, the rising temperature effect outweighs somewhat, so that the apparent irreversible degradation can be slightly smaller than the real one.

Therefore, based on these data, a voltage–temperature model is going to be elaborated, to distinguish between long-term degradation and superimposing effects resulting from temperature variations.

## 4. Conclusions

The influence of air contaminants on PEM fuel cells operated under real outdoor conditions has been investigated in a field study for a period of over 4500 h at three different locations with different levels of air contamination. Operation under these conditions showed highest time-averaged cell voltages at the location with the lowest levels of air pollution and vice versa, thus establishing a negative correlation between average air impurity concentrations and average cell voltage levels.

Periodic daily variations of the cell voltages could be observed and correlated with the periodic daily variations of temperature, on the one hand, and of air contaminant concentrations, on the other hand. Here, a different behavior for different locations and operation points could be observed: At the lowest polluted location, all cell voltages varied concordantly with the ambient temperature. However, at the location with the highest levels of air contamination, the behavior of the cell voltages differed with the operation point: At low current densities, the voltage variations were caused by variations of the pollutant concentrations, whereas at larger current densities the voltage variations could be attributed to temperature variations. This could be explained by the increased temperature sensitivity of the cell voltage at larger current densities due to the influence of temperature on the water content of the cell.

## Acknowledgments

The authors would like to thank for the financial support by the German Federal Ministry of Education and Research (BMBF, FKZ 16SV3390). Special thanks also to the Deutscher Wetterdienst DWD, the Landesanstalt für Umwelt, Messungen und Naturschutz Baden-Württemberg LUBW and the Umweltbundesamt UBA for supplying the weather and pollutant data and providing the location for the test platforms. The author N. Zamel would like to acknowledge the financial support by the Natural Sciences and Engineering Research Council of Canada (NSERC) in the form of a Postdoctoral Fellowship.

## References

[1] R. Mohtadi, W.-K. Lee, J.W. Van Zee, J. Power Sources 138 (2004) 216–225.
[2] D. Yang, J. Ma, L. Xu, M. Wu, H. Wang, Electrochim. Acta 51 (2006) 4039–4044.
[3] J. Wu, X.Z. Yuan, J.J. Martin, H. Wang, J. Zhang, J. Shen, S. Wu, W. Merida, J. Power Sources 184 (2008) 104–119.
[4] J. St-Pierre, N. Jia, R. Rahmani, J. Electrochem. Soc. 155 (2008) B315–B320.
[5] Felix N. Büchi, Minoru Inaba, Thomas J. Schmidt (Eds.), Polymer Electrolyte Fuel Cell Durability, Springer, 2009.
[6] H. Mahzoul, J.F. Brilhac, P. Gilot, Appl. Catal. B 20 (1999) 47–55.
[7] W. Huang, Z. Jiang, J. Jiao, D. Tan, R. Zhai, X. Bao, Surf. Sci. Lett. 506 (2002) L287–L292.
[8] R. Borup, E. Brosha, F. Garzon, B. Pivovar, T. Rockward, T. Springer, F. Uribe, I. Urdampilleta, J. Valerio, in: DOE hydrogen, fuel cells and infrastructure technologies 2007 kickoff meeting.
[9] F. Jing, M. Hou, W. Shi, J. Fu, H. Yu, P. Ming, B. Yi, J. Power Sources 116 (2007) 172–176.
[10] S. Knights, N. Jia, C. Chuy, J. Zhang, Fuel Cell Seminar: Fuel Cell Progress, Challenges and Markets, Palm Springs, California, 2005.
[11] A. Baltes, Verkehrsstärken an ausgewählten Spotmessstellen, Landesanstalt für Umwelt, Messungen und Naturschutz, Baden-Württemberg, 2009.
[12] A. Baltes, Deutscher Wetterdienst, www.dwd.de.
[13] Messstation Schauinsland, www.umweltbundesamt.de/luft/luftmessnetze/stationen/schau/index.htm.